Electronic Supplementary Information

Co_3O_4 nanosheets as the high-performance catalyst for oxygen evolution proceeding *via* the twice two-electron process

Shichao Du,[a] Zhiyu Ren,[b]* Yang Qu,[b] Jun Wu,[b] Wang Xi,[b] Jiaqing Zhu[b] & Honggang Fu[a, b] *

[a] *Institute of Theoretical Chemisty, JiLin University, 130023 ChangChun P. R. China.*

[b] *Key Laboratory of Functional Inorganic Material Chemistry, Ministry of Education of the People's Republic of China; School of Chemistry and Materials Science, Heilongjiang University, 150080 Harbin P. R. China.*

Tel: +86-451-86604330;

Fax:+86-451-86661259;

E-mail address: fuhg@vip.sina.com; zyren@hlju.edu.cn.

1. Experimental Section

1.1 Materials

$Co(NO_3)_2 \cdot 6H_2O$ were obtained from Beijing Chemical Reagents. Ethanol and toluene were obtained from Longxi Chemical Corp. Oleylamine (OAm) (99%) was obtained from Aladdin Chemistry Co. All of the reagents and solvents were analytical grade and used as received without further purification.

1.2 Preparation of materials

Synthesis of Co^{2+}-OAm complex by phase-transfer process.

In a typical procedure, 0.2 mmol $Co(NO_3)_2 \cdot 6\ H_2O$ was dissolved in 20 mL deionized water, then 20 ml ethanol containing OAm (3.5 $mmol \cdot L^{-1}$) was added. After sufficient mixing, the Co^{2+}-OAm complex was formed. Afterwards, 20 mL toluene was added and stirred for 5 mins. The mixture was then transferred to a separatory funnel and stationary for 1 h to separate water and toluene. At last, the Co^{2+}-OAm dissolved in toluene (the upper layer) was separated and used in next step.

Synthesis of Co_3O_4 NSs, Co_3O_4 NPs and calcinated Co_3O_4 NSs.

The prepared Co^{2+}-OAm complex in toluene was transferred into a three-necked bottle with sustained O_2 bubble to keep the oxygen enrichment environment. After the solution was heated to 50 °C and kept, the aqueous of $NaBH_4$ (0.01 $mol \cdot L^{-1}$) was added dropwise. The molar ratio of $NaBH_4$ and Co^{2+}-OAm was about 5:1. The reaction was held at 50 °C for 2 h. After reaction, the brown products precipitated into the aqueous layer were separated by using vacuum filtration. After washing with water and ethanol several times, the free-standing ultrathin Co_3O_4 NSs were obtained. The Co_3O_4 NPs was prepared by the similar produce, except that the reaction was held at 0 °C for 5 h. The calcinated Co_3O_4 NSs were obtained by thermal-treatment of Co_3O_4 NSs at 300 ºC in air for 2 h.

1.3 Electrochemical Measurements

Electrochemical experiments were performed on an electrochemical workstation (BAS 100B, USA). A standard three-electrode cell was employed, using a saturated calomel electrode (SCE, saturated KCl-filled) and a Pt wire as the reference and the counter electrode, respectively. A rotating disk electrode (RDE-2, BAS USA) and a glassy carbon electrode (GCE) with 3 mm diameter were used as working electrodes for OER and H_2O_2 oxidation, respectively. 5 mg of catalyst dispersed in 200 μL mixed solution containing 20 μL of 5 wt.% Nafion ionomer and 180 μL of alcohol. After the catalyst ink was sonicated for at least 30 min, about 5 μL of the catalyst ink was evenly covered onto the RDE or GCE electrode surface and allowed to dry at ambient temperature.

Before measuring, each working electrode was cycled 20-100 times by cyclic voltammetry (CV, at a scan rate of 100 $mV \cdot s^{-1}$) in electrolyte (1 M KOH), until a stable CV curve was obtained. The polarization curves were converted from linear sweep voltammetry (LSV, 100% *iR*-compensation correction) was kept the scan rate at 5 $mV \cdot s^{-1}$. Chronopotentiometry was performed under a serial constant current density of 10 $mA \cdot cm^{-2}$, controlled by a VersaSTAT 3 electrochemistry workstation. To gain insight into the reaction mechanism, the rotating ring-disk electrode (RRDE, Pine Research Instrumentation, USA) curves were measured in 0.1 M KOH solution (N_2-saturated). The potentials on the Pt ring electrode were set as 1.2 V and 0.6 V *vs.* RHE for detecting HO_2^- and O_2 produced at the disk electrode, respectively. To evaluate the activity of the catalyst towards H_2O_2 oxidation, H_2O_2 (30 vol%) solution was used for electrochemical measurements. OER performance tests involving RDE and RRDE were carried out with the working electrode continuously rotating at 1600 rpm to get rid of the oxygen bubbles. All the tests were carried out at room temperature (about 25 °C).

The Tafel slope was calculated from the Tafel equation as follows $\eta = b \times log(j/j_0)$, where η is the overpotential, b is the Tafel slope, j is the current density, and j_0 is the exchange current density. [S1]

1.4 Characterization

The scanning electron microscopy (SEM with an acceleration voltage of 15 kV and the energy dispersive X-Ray spectroscopy (EDX, Hitachi S-4800) was used to observe the morphologies and the elementary composition. The transmission electron microscopy (TEM, JEOL JEM-3010) with an acceleration voltage of 300 kV was employed as the morphology of the products (carbon-coated copper grids were used as sample holders for TEM analysis). Chemical compositions of the samples were checked by X-ray photoelectron spectroscopy (XPS, AXIS UL TRA DLD). X-ray diffraction (XRD) patterns were obtained by a Bruker D8 ADVANCE diffractometer by using Cu Kα radiation (λ = 1.5406 Å). The Raman spectra were recorded with a Raman spectrophotometer (HR800, HORIBA Jobin Yvon Company, the laser with 457.9 nm wavelength). The specific surface area of the samples was calculated by Brunauer-Emmett-Teller (BET) equation performed by Nitrogen adsorption-desorption isotherms at 77 K (Micromeritics Tristar II 3020 nitrogen adsorption apparatus).

2. Results and discussion

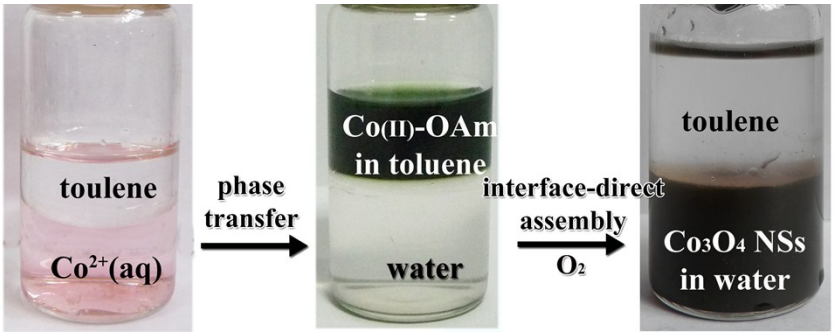

Fig. S1 The photos of the synthesis process of Co_3O_4 NSs.

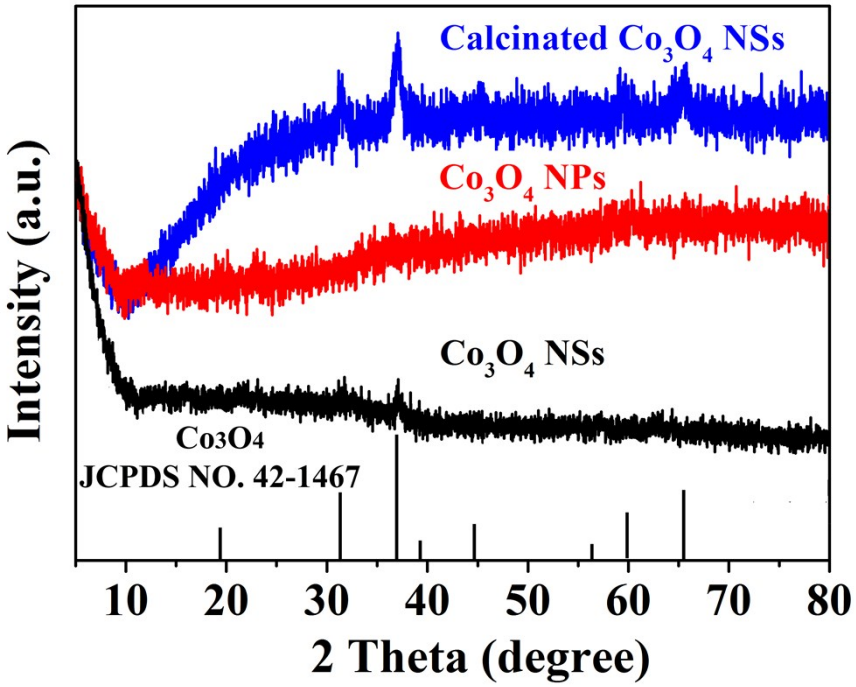

Fig. S2 XRD patterns of Co_3O_4 NSs, Co_3O_4 NPs and calcinated Co_3O_4 NSs.

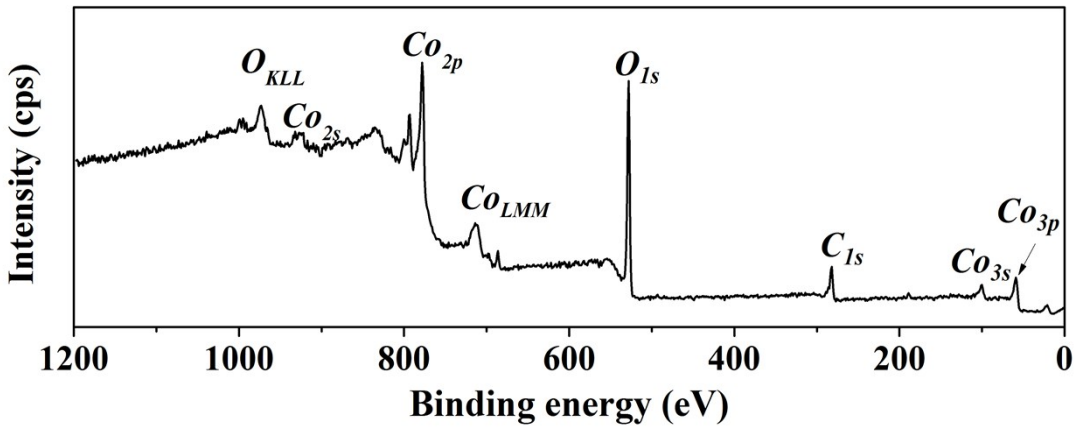

Fig. S3 The XPS spectrum of Co_3O_4 NSs.

Table S1 The element analyst of Co_3O_4 NSs obtained by EDX and XPS.

Method	Element (at%)			
	Co	O	N	C
XPS	32.22	47.69	0.23	19.86
EDX	35.83	55.23	0	8.94

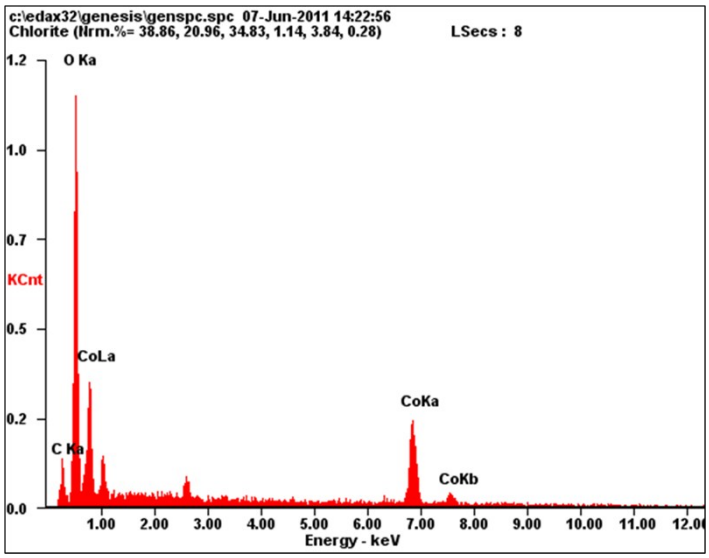

Fig. S4 EDX spectrum of Co_3O_4 NSs.

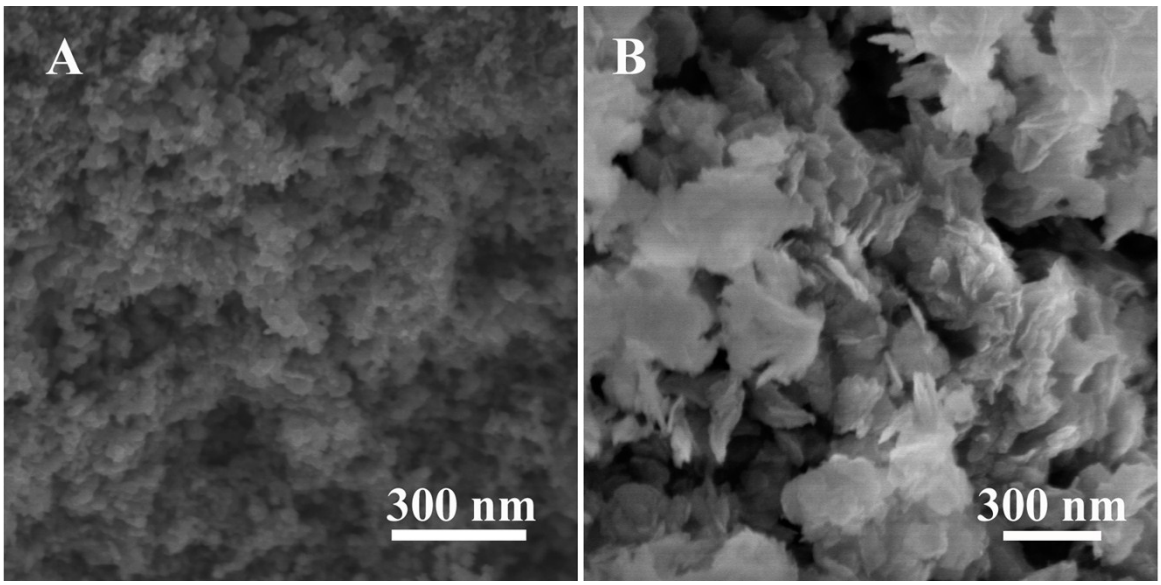

Fig. S5 The SEM images of Co_3O_4 NPs (A) and calcinated Co_3O_4 NSs (B).

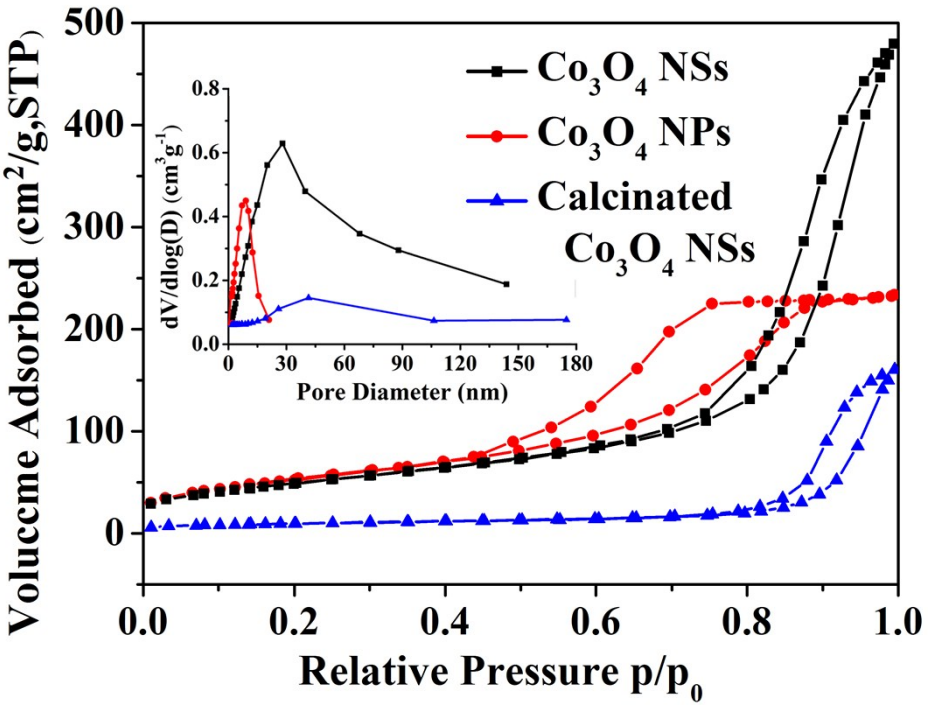

Fig. S6 Nitrogen adsorption-desorption isotherms and pore-size distribution curves (inset) of Co_3O_4 NSs, Co_3O_4 NPs and calcinated Co_3O_4 NSs.

Table S2. Comparison of BET surface area and pore diameter of Co_3O_4 NSs, Co_3O_4 NPs and calcinated Co_3O_4 NSs.

Sample name	BET Surface area ($m^2 \cdot g^{-1}$)	Pore diameter (nm)
Co_3O_4 NSs	191.2	28.2
Co_3O_4 NPs	183.5	8.5
Calcinated Co_3O_4 NSs	36.7	41.7

The electrochemical surface area (ECSA), estimated from the electrochemical double-layer capacitance (C_{dl}), is one of important factors for the electrochemical performance.[S2, S3] The CVs of various catalysts were studied in the region of 0.15-0.25 V, in which the current response was only derived from the charging of the C_{dl} (Fig. S7). According to the linear slope of capacitive current *vs.* scan rate,[S4, S5] the capacitance of the three samples decrease in the order of Co_3O_4 NSs (49 mF·cm^{-2}) > Co_3O_4 NPs (22 mF·cm^{-2}) > calcinated Co_3O_4 NSs (7 mF·cm^{-2}) (Fig. 2A). Apparently, the loose, porous Co_3O_4 NSs with low crystallization have more effective surface areas (electroactive sites) than Co_3O_4 NP and calcinated Co_3O_4 NSs, and thus the highest catalytic activity for OER.

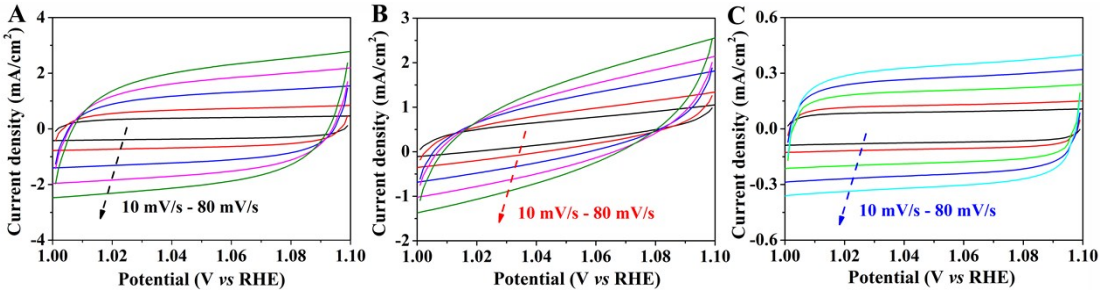

Fig. S7 (A-C) CVs for Co_3O_4 NSs, Co_3O_4 NPs, and calcinated Co_3O_4 NSs at various scan rate (10, 20, 40, 60 and 80 mV·s^{-1})

Table S3. Four parameters defined for OER activity of Co_3O_4 NSs, Co_3O_4 NPs and calcinated Co_3O_4 NSs.

Samples	Onset potential	Tafel plots (mV·dec^{-1})	Current density (overpotential at 300 mV)	Potential (j = 10 mA·cm^{-2})
Co_3O_4 NSs	1.51 V	69	3.6 mA/cm^2	1.56 V
Co_3O_4 NPs	1.54 V	96	1.7 mA/cm^2	1.61 V
calcinated Co_3O_4 NSs	1.51 V	85	1.2 mA/cm^2	1.59 V

Table S4 Comparison of catalytic performance of Co_3O_4 NSs to some reported Co-based catalysts.

Materials	Onset potential (V vs RHE)	Potential (at 10 mA·cm^{-2}, V vs RHE)	Tafel slope (mV/dec)	Ref
NiCo LDH/CP [1]	1.535	1.597	40	S6
Exfoliated CoCo LDH	1.535	1.583	45	S7
Exfoliated NiCo LDH	1.515	1.564	41	
NiCo LDH NTAs [2]	1.540	1.690	65	S8
Ni NTAs [2]	1.604	1.890	145	
NG-NiCo LDH [3]	1.580	1.63 (at 145.3 mAcm^{-2})	614	S9
CoNi LDH	1.590	1.640 (at 5 mAcm^{-2})	---	S10
CoNi LDHs	1.623	1.720 (at 1 mAcm^{-2})	---	S11
CoCo LDHs	1.638	1.840	---	
NiCo LDH/Ni foam	1.520	1.650	113	S12
ZnCo LDH	1.570	---	---	S13
CoMn LDH	1.500	1.554	43	S14
NiCoFe LDH	1.46	---	53	S15
CoO/N-CG[4]	---	1.570	71	S16
$NiCo_2O_4$ HNSs [5]	1.500	1.590	64.4	S17
PNG-$NiCo_2O_4$[6]	1.540	---	156	S18
NG-$NiCo_2O_4$	1.570	---	249	
$NiCo_2O_4$ NSs[7]	1.550	---	30	S19
$Ni_{0.6}Co_{2.4}O_4$/Ni foil	1.570	1.760		S20
Co_3O_4/N-rGO	---	1.540	67	S21
CoNi LDH/CoO NSs	1.480	1.530	123	S22
Co_3O_4-CNT	1.51	1.62	65	S23
Co_3O_4@/NMC-CNT[8]	1.50	1.55	62	S24
Co_3O_4 Nanocubes/N-rGO	1.45	1.51	69	S25
Co_3O_4 NSs	***1.510***	***1.560***	***69***	***This work***

[1] CP, abbreviation for carbon paper;
[2] NTAs, abbreviation for nanotube arrays;
[3] NG, abbreviation for N doped graphene;
[4] N-CG, abbreviation for nitrogen doped hollow crumpled grapheme;
[5] HNSs, abbreviation for hollow nanosponges;
[6] PNG, abbreviation for 3D hybrid film of porous N-doped graphene;
[7] NSs, abbreviation for nanosheets;
[8] NMC, abbreviation for N-doped mesoporous carbon layer.

The RRDE technique was used for confirm the intermediate products formed on Co_3O_4 NSs catalyst surface during OER process. In general, OER on catalysts could carry out a four-electron step to form O_2, or a two-electron pathway to form H_2O_2 as the intermediate product before the oxygen evolution. The Pt ring electrode potentials of 1.20 V and 0.60 V are applied to detect the H_2O_2 and O_2, respectively, at a scan potential ranging of the disk from 1.2 to 1.8 V.[S22] As shown in Fig. S8, when the Pt ring electrode potential is 1.20 V, a microamp-scale oxidation current is recorded (red line), implying negligible production of hydrogen peroxide in the system. Instead, an apparent oxygen reduction reaction (ORR) current was obtained at a Pt ring electrode potential of 0.60 V.

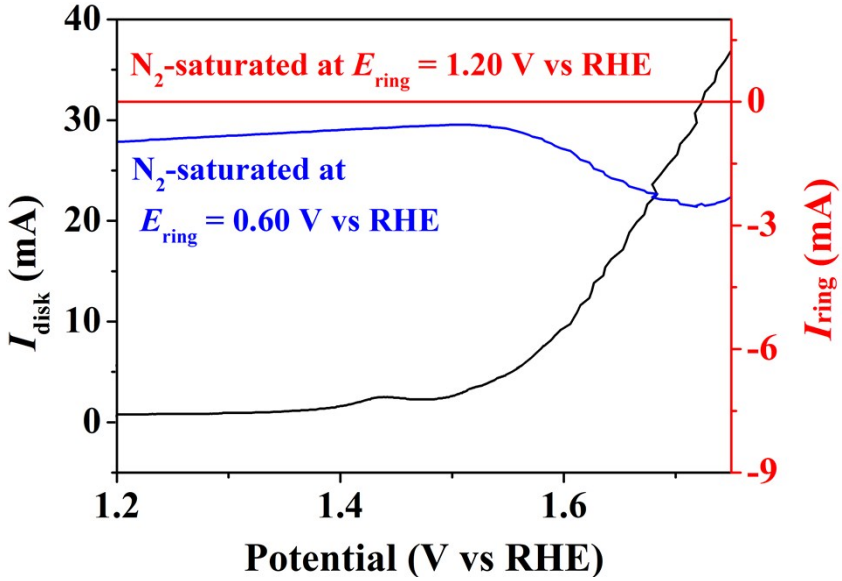

Fig. S8 RRDE measurement of ring current density recorded at the Pt ring electrode maintained at 1.2 or 0.6 V (vs. RHE) in N_2-saturated 1.0 M KOH solution and the related current density at the Co_3O_4 NSs disk electrode (rotation speed: 1600 rpm, scan rate: 5 $mV \cdot s^{-1}$).

To further evaluate the catalytic activity of Co_3O_4 NSs towards H_2O_2 oxidation, the typical amperometric response of Co_3O_4 NSs to the successive addition of different amounts of H_2O_2 into the stirring 1 M KOH is recorded at 1.45 V *vs.* RHE (as shown in Fig. S9A). With the concentration of H_2O_2 increases, the electrochemical response of Co_3O_4 NSs displays a typical staircase curve. The Co_3O_4 NSs activity in the reaction with H_2O_2 can be

described by the calibration curve in Fig. S9B. The increases of the current density is proportional to the H_2O_2 concentrations, and two linear response for H_2O_2 are expressed as: (1) I (μA) = 2.27 (mA·μM^{-1}) C (μM, H_2O_2) + 10.28 (μA) (5-71 μM, R^2 = 0.997, blue line); (2) I (μA) = 0.68 (μA·μM^{-1}) C (μM, H_2O_2) + 109.24 (μA) (80-700 μM, R^2 = 0.993, red line). Derived from the calibration curve, the electrochemical response of Co_3O_4 NSs towards H_2O_2 can reach as low as 16.9 μM/cm^2 (S/N = 3). The results suggest that Co^{III}/Co^{IV} redox couple formed at 1.45 V *vs.* RHE can facilitate H_2O_2 oxidation.

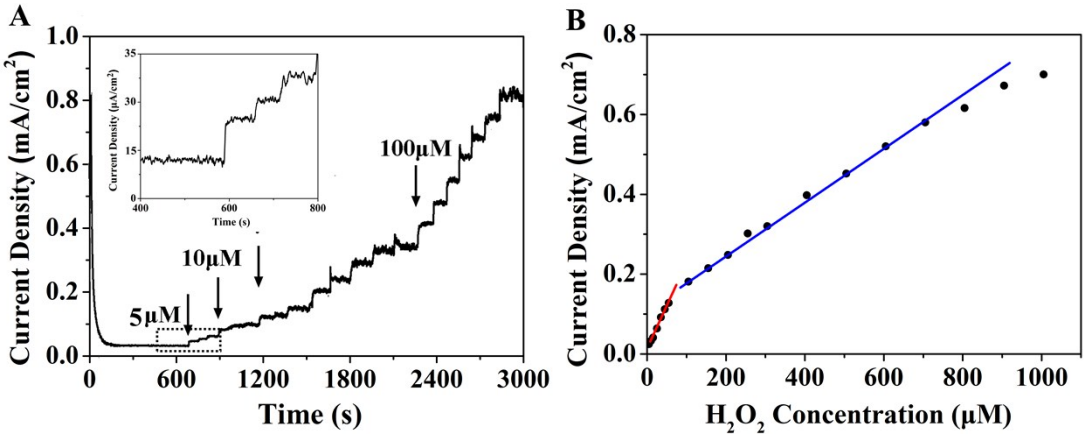

Fig. S9 (A) I–t curve of Co_3O_4 NSs on GCE (holding at 1.45 V *vs.* RHE) for the successive addition of H_2O_2 in 1 M KOH (insert is the partial enlargement); (B) the linear calibration relationship of current *vs.* H_2O_2 concentration (insert is the partial enlargement).

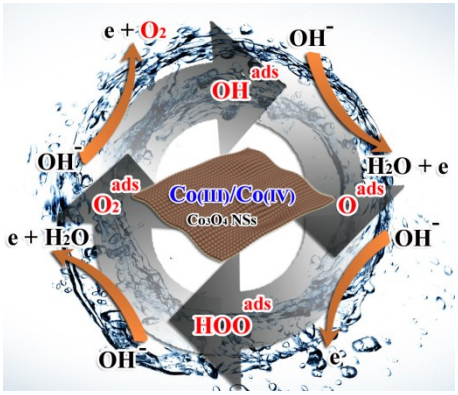

Fig. S10 The schematic illustration of the proposed catalytic mechanism of Co_3O_4 NSs towards OER.

The electrocatalytic activity of Co_3O_4 NSs towards H_2O_2 was also studied. To assess the reaction kinetics properties, CVs of Co_3O_4 NSs at different scan rates (from 5-100 $mV \cdot s^{-1}$) are shown in Fig. S11A. In the CVs, the obvious pair of redox peaks, the cathodic peak (i_{pc}) at about 1.45 V *vs.* RHE and the anodic peak (i_{pa}) at about 1.4 V *vs.* RHE, are also associated to the electrochemical transformation of Co^{III}/Co^{IV} (1.2 *vs.* RHE and 1.15 *vs.* RHE are attribute to Co^{II}/Co^{III}). With an increase of the scan rate, the cathodic and anodic peak currents are increase. Apparently, the relationship between the peak currents of Co^{III}/Co^{IV} (both i_{pa} and i_{pc}) and the square root of the scan rate ($v^{1/2}$) can be evaluated by the series linear plots (shown in Fig. S11B). The calibration plots can be described by eqn (S1.1) and eqn (S1.2). According to the characteristic indexes of the heterogeneous electron transfer reactions, the electron transfer kinetics of the Co_3O_4 NSs is controlled by diffusion confinement.

$$i_{pa} = 4.49\ v^{1/2} - 5.48 \quad (R^2 = 0.997) \qquad \text{(S1.1)}$$

$$i_{pc} = -3.28\ v^{1/2} + 2.52 \quad (R^2 = 0.998) \qquad \text{(S1.2)}$$

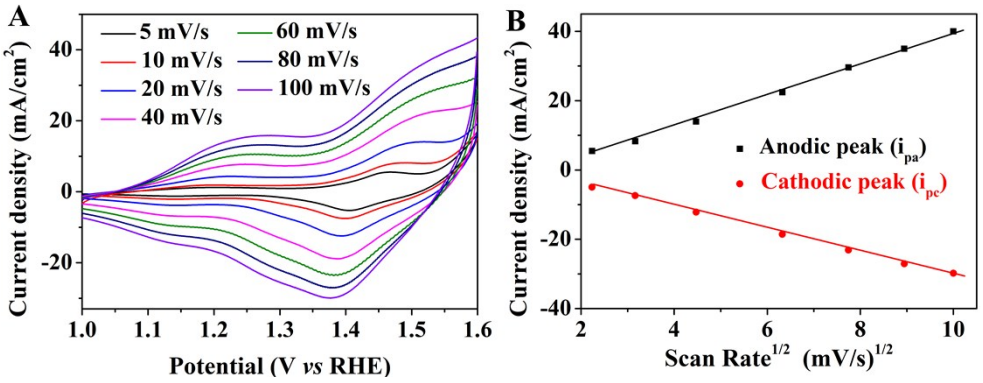

Fig. S11 (A) CVs of Co_3O_4 NSs on GCE in 1 M KOH solution (pH = 13.8) measured at different scan rates (5-100 $mV \cdot s^{-1}$); (B) the linear calibration relationship between the anodic (black line) and cathodic (red line) peak currents and the square root of the scan rate.

Additional notes and references:

S1 Schultze J. W. Sergio Trasatti (Ed.): Electrodes of Conductive Metallic Oxides, Part A. *Elsevier Scientific Publishing Company,* Amsterdam, New York 1980.

S2 S. Trasatt, O. A. Petri, *Pure Appl. Chem.*, 1991, **63(5)**, 711 – 734.

S3 H. J. Yan, C. G. Tian, L. Wang, A. Wu, H. G. Fu, *Angew. Chem. Int. Ed.,* 2015, **54**, 6325-6329.

S4 F. Song and X. Hu, *Nat. Commun.*, 2014, **5**, 0447.

S5 M. A. Lukowski, S. A. Daniel, F. Meng, A. Forticaux, L. Li, and S. Jin, *J. Am. Chem. Soc.,* 2013, **135**, 10274–10277.

S6 H. F. Liang, F. Meng, M. Cabán-Acevedo, L. S. Li, A. Forticaux, L. C. Xiu, Z. C. Wang and S. Jin, *Nano Lett.,* 2015, **15**, 1421-1427.

S7 F. Song and X. L.Hu, *Nat. Comm.,* 2014, **5**, 4477.

S8 Z. L. Zhao, H. X. Wu, H. L. He, X. L. Xua and Y. D. Jin, *Adv. Funct. Mater.,* 2014, **24**, 4698-4705.

S9 S. Chen, J. J. Duan, M. Jaroniec and S. Z. Qiao, *Angew. Chem. Int. Ed.,* 2013, **52**, 13567-13570.

S10 R. Valdez, D. B. Grotjahn, D. K. Smith, J. M. Quintana and A. Olivas, *Int. J. Electrochem. Sci.,* 2015, **10**, 909-918.

S11 Y. Zhang, B. Cui, C. S. Zhao, H. Lin and J. B. Li, *Phys. Chem. Chem. Phys.* 2013, **15**, 7363-7369.

S12 J. Jiang, A. L. Zhang, L. L. Li and L. H. Ai, *J. Power Sources,* 2015, **278**, 445-451.

S13 X. X. Zou, A. Goswami and T. Asefa, *J. Am. Chem. Soc.,* 2013, **135**, 17242-17245.

S14 F. Song and X. L. Hu, *J. Am. Chem. Soc.,* 2014, **136**, 16481-16484.

S15 Q. Yang, T. Li, Z. Y. Lu, X. M. Sun and J. F. Liu, *Nanoscale,* **2014**, 6, 11789-11794.

S16 S. Mao, Z. H. Wen, T. Z. Huang, Y. Hou and J. H. Chen, *Energy Environ. Sci.,* 2014, **7**, 609-616.

S17 C. Z. Zhu, D. Wen, S. Leubner, M. Oschatz and W. Liu, *Chem. Commun.,* 2015, **51**, 7851-7854.

S18 S. Chen and S. Z. Qiao, *ACS Nano,* 2013, **7**, 10190-10196.

S19 J. Bao, X. D. Zhang, B. Fan, J. J. Zhang, M. Zhou, W. L. Yang, X. Hu, H. Wang, B. C. Pan and Y. Xie, *Angew. Chem. Int. Ed.,* 2015, **54**, 7399-7404.

S20 T. N. Lambert, J. A. Vigil, S. E. White, D. J. Davis, S. J. Limmer, P. D. Burton, E. N. Coker, T. E. Beecheme and M. T. Brumbach, *Chem. Commun.,* 2015, **51**, 9511-9514.

S21 Y. Liang, Y. G. Li, H. L. Wang, J. G. Zhou, J. Wang, T. Regier and H. J. Dai, *Nat. Mater,*. 2011, **10**, 780-786.

S22 J. Wu, Z. Y. Ren, S. C. Du, L. J. Kong, B. W. Liu, W. Xi, J. Q. Zhu and H. G. Fu, *Nano Research.* 2016, DOI 10.1007/s12274-015-0950-4.

S23 X. Y. Lu and C. Zhao, *J. Mater. Chem. A.*, 2013, **1**, 12053-12059.

S24 X. Z. Li, Y. Y. Fang, X. Q. Lin, M. Tian, X. C. An, Y. Fu, R. Li, J. J. and J. T. Ma, *J. Mater. Chem. A.*, 2015, **3**, 17392-17402.

S25 S. K. Singh, V. M. Dhavale and S. Kurungot, *ACS Appl. Mater. Interfaces*, 2015, **7**, 442-451.